Science of the Total Environment 788 (2021) 147773

Contents lists available at ScienceDirect

Science of the Total Environment

journal homepage: www.elsevier.com/locate/scitotenv

The anaerobic oxidation of methane in paddy soil by ferric iron and nitrate, and the microbial communities involved

Dan Luo [a,b,c], Xiangtian Meng [a,b,c], Ningguo Zheng [a,b,c], Yaying Li [a,b], Huaiying Yao [a,b,d,*], Stephen J. Chapman [e]

[a] Key Laboratory of Urban Environment and Health, Institute of Urban Environment, Chinese Academy of Sciences, Xiamen 361021, People's Republic of China
[b] Zhejiang Key Laboratory of Urban Environmental Processes and Pollution Control, Ningbo Urban Environment Observation and Research Station-NUEORS, Institute of Urban Environment, Chinese Academy of Sciences, Ningbo 315800, People's Republic of China
[c] University of Chinese Academy of Sciences, Beijing 100049, People's Republic of China
[d] Research Center for Environmental Ecology and Engineering, School of Environmental Ecology and Biological Engineering, Wuhan Institute of Technology, Wuhan 430073, People's Republic of China
[e] The James Hutton Institute, Craigiebuckler, Aberdeen AB15 8QH, UK

HIGHLIGHTS

- Fe^{3+} and NO_3^- can stimulate the anaerobic oxidation of methane (AOM) process.
- Biochar has no obvious effect on the AOM process.
- Iron/nitrate-reducing bacteria are active microorganisms involved in the AOM process.
- Electron acceptors coupled with AOM is a key process to reduce methane emissions.

GRAPHICAL ABSTRACT

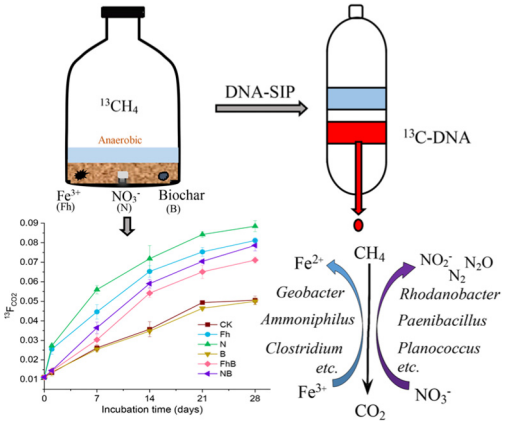

ARTICLE INFO

Article history:
Received 2 March 2021
Received in revised form 11 May 2021
Accepted 12 May 2021
Available online 15 May 2021

Editor: Frederic Coulon

Keywords:
Anaerobic oxidation of methane
Paddy soil
Electron acceptors
Microbial communities

ABSTRACT

The anaerobic oxidation of methane (AOM) mediated by microorganisms is a key process in the reduction of methane emissions, and AOM-coupled electron acceptors have been shown to regulate methane emissions into the atmosphere in marine systems. Paddy fields are a significant source of methane and account for 20% of global methane emissions, but the effect of electron acceptors on the methane emission process in flooded paddy fields has been poorly characterized. This study aimed to determine whether the electron acceptors ferric iron and nitrate, and biochar, acting as an electron shuttle, can regulate the AOM process in paddy soil, with or without interaction between biochar and these two electron acceptors. We also aimed to characterize which microorganisms are actively involved. Here, we added ^{13}C-labeled CH_4 ($^{13}CH_4$) into anaerobic microcosms to evaluate the role of electron acceptors by measuring the methane oxidation rate and the enrichment of ^{13}C-labeled CO_2 ($^{13}CO_2$). We then combined DNA-stable isotope probing with amplicon sequencing to study the active microorganisms. We found for the first time that, in addition to nitrate, ferric iron can also effectively promote AOM in paddy soil. However, there was no significant effect of biochar. Ferric iron-dependent AOM was mainly carried out by iron-reducing bacteria (*Geobacter*, *Ammoniphilus* and *Clostridium*), and nitrate-dependent AOM was mainly by nitrate-reducing bacteria (*Rhodanobacter*, *Paenibacillus* and *Planococcus*). Our results demonstrate

* Corresponding author at: Ningbo Urban Environment Observation and Research Station-NUEORS, Institute of Urban Environment, Chinese Academy of Sciences, Ningbo 315800, Zhejiang Province, People's Republic of China.
E-mail address: hyyao@iue.ac.cn (H. Yao).

https://doi.org/10.1016/j.scitotenv.2021.147773

that the AOM process, regulated by the electron acceptors ferric iron and nitrate, can alleviate methane emission from paddy soil. The potentially active microorganisms related to electron acceptor reduction may be crucial for this methane sink and deserve further research.

1. Introduction

Methane is a major greenhouse gas, which has 28 times the warming effect of carbon dioxide on a mass basis and has contributed 20% to global warming over the past 100 years (Pachauri et al., 2014). The anaerobic oxidation of methane (AOM) mediated by microorganisms is a critical process that regulates the global climate by reducing methane emissions (Niemann et al., 2006; Bar-Or et al., 2017). Methane is consumed by the AOM process in many natural ecosystems before it is released into the atmosphere (Knittel and Boetius, 2009; Cai et al., 2018). Therefore, AOM is regarded as a gatekeeper of the methane balance and the global carbon cycle (Segarra et al., 2015). In addition to nutrients, the supply of electron acceptors is considered to be the main limiting factor for methane oxidation under anaerobic conditions (Song et al., 2019).

Several electron acceptors involved in the AOM process have been discovered over time, including sulfate, nitrate, and, controversially, ferric iron. Sulfate was for many years considered to be the only final electron acceptor in the AOM process with anaerobic methanotrophic archaea (ANME) and sulfate-reducing bacteria as the key microorganisms (Reeburgh, 1976; Knittel and Boetius, 2009). However, a variety of other electron acceptors, especially nitrate (Davies, 1973; Caldwell et al., 2008) and ferric iron (Ettwig et al., 2016) are thermodynamically more favorable electron acceptors than sulfate (Eqs. (1)–(3)):

$$5CH_4 + 8NO_3^- + 8H^+ \rightarrow 5CO_2 + 4N_2 + 14H_2O\ \Delta G^{0\prime} = -765\ \text{kJ mol}^{-1}\ CH_4; \quad (1)$$

$$CH_4 + 8Fe^{3+} + 2H_2O \rightarrow CO_2 + 8Fe^{2+} + 8H^+\ \Delta G^{0\prime} = -454\ \text{kJ mol}^{-1}\ CH_4; \quad (2)$$

$$CH_4 + SO_4^{2-} \rightarrow HCO_3^- + HS^- + H_2O\ \Delta G^{0\prime} = -17\ \text{kJ mol}^{-1}\ CH_4. \quad (3)$$

In anoxic freshwater sediments where sulfate is largely absent, nitrate can act as an electron acceptor for AOM, where methane is converted into carbon dioxide through the reverse methanogenesis pathway and denitrifying bacteria obtain electrons to complete denitrification (Raghoebarsing et al., 2006). Hu et al. (2014) used stable isotope and 16S rRNA sequencing to explore the nitrite-dependent AOM process in freshwater wetlands and found that this process may be important as a global methane sink. At first, several reports showed that iron has a certain inhibitory effect on the methanogenic activities of flooded soils (Achtnich et al., 1995; Lueders and Friedrich, 2002). Later, some studies have shown that microbes can use ferric iron (ferrihydrite) in wetland sediments as an electron acceptor to oxidize methane (Norði et al., 2013; Segarra et al., 2013). Ferric iron-dependent AOM was demonstrated in basin seep sediments by the finding that methanotrophic ANME-2 archaea could respire electron donors via the reduction of ferric iron (Scheller et al., 2016). Recently, Leu et al. (2020) demonstrated that *Methanoperedenaceae* is capable of AOM coupled to manganese reduction. In addition, arsenic is also considered an overlooked partner of AOM in wetland soils (Shi et al., 2020). Hence, AOM coupled to different electron acceptors is critical for regulating methane emissions in various anaerobic environments.

Paddy fields account for about one-fifth of the global methane emissions from anthropogenic sources. China produces more methane from paddy fields than any other country in the world (Yan et al., 2009) and emissions were estimated to be 4.75 Tg in 2015 (Sun et al., 2020). A better understanding of the AOM process may help to reduce the negative impact of methane emissions. Additionally, as a specially constructed wetland ecosystem, subject to alternating dry and wet cycles, flooded paddy field has a typical redox gradient. Hence it is an ideal model for studying the electron transport process of AOM. The reduction of nitrate linked to AOM in paddy soils has been well-established (Vaksmaa et al., 2017). The reduction of ferric iron coupled to methane oxidation has been demonstrated in freshwater sediments (Sivan et al., 2011), brackish coastal sediments (Egger et al., 2015), Amazonian floodplain (Gabriel et al., 2020) and mixed liquid culture (He et al., 2019). However, a controversy exists about whether ferric iron can effectively promote the AOM process in paddy soil and the results so far are unclear (Fan et al., 2020).

Biochar is a solid product obtained by the thermochemical conversion of straw, manure, and other biomass under oxygen-limited conditions. In recent years, biochar has served as an increasingly popular soil amendment, widely used in paddy soil as it can improve soil fertility and water retention capacity (Batool et al., 2015). Saquing et al. (2015) reported that biochar can act as an electron acceptor and can promote the respiration of microorganisms in an anaerobic reactor, oxidizing acetate and promoting the reduction of nitrate. By adding different amounts of biochar to an anaerobic digester, it was found that biochar can increase the production of methane, but excessive biochar decreased the content of methane (Li et al., 2019a). Biochar can act as an electron shuttle due to its quinone and aromatic structures (Keiluweit et al., 2010), participate in redox reactions mediated by microorganisms, and have an important impact on the soil biogeochemical cycle. Qiao et al. (2017) found that the electron shuttle function of biochar can stimulate the proliferation of the arsenic-respiring bacteria *Geobacter* in anaerobic paddy soil and promote arsenic reduction. The fact that biochar can participate in interspecies electron transfer processes (Chen et al., 2014), suggests that it can, like ferric iron and nitrate, also act as an electron acceptor to regulate AOM. However, Fan et al. (2020) found that paddy soil treated with biochar had reduced AOM compared to the control soil. Hence it is uncertain whether biochar can act as an electron acceptor to regulate AOM in paddy soil and whether it can interact with the reduction of ferric iron and nitrate during AOM.

The role that electron acceptors play is crucial to understanding the AOM process. However, studies about the relationship between the reduction of ferric iron and the AOM process are controversial, and our knowledge about the active microorganisms that employ electron acceptors (ferric iron, nitrate, or biochar) coupled to AOM, particularly within paddy soil, is still rudimentary. DNA Stable-Isotope Probing (DNA-SIP) technology has the advantage of circumventing the shortcomings of traditional cultivation method and facilitates the identification of target microorganisms by tracking the labeled substrate (Martinez-Cruz et al., 2017; Li et al., 2019b; Zhang et al., 2020). In this study, a microcosm experiment with ^{13}C-labeled CH_4 ($^{13}CH_4$) was conducted. AOM rates and ^{13}C-labeled CO_2 ($^{13}CO_2$) enrichment were determined, and DNA-SIP combined with high-throughput sequencing was used to probe the functioning microbes with different electron acceptors. The objectives of this paper were 1) determine whether the reduction of iron is coupled with the AOM process to reduce methane emissions in paddy soil; 2) to probe the microbial players in ferric iron-dependent and nitrate-dependent AOM; 3) to explore the effects of biochar on the AOM process and whether it can promote ferric iron-dependent and nitrate-dependent AOM.

2. Materials and methods

2.1. Sample collection and chemical analysis

In September 2018, paddy soil samples were taken from the surface layer in a rice-wheat rotation field near Ningbo city, Zhejiang province in China (29°47′24″N, 121°22′3″E), which is characterized by a typical subtropical monsoon climate. Sampling methods were described in detail previously (Zhu et al., 2020). We randomly selected three 5 × 5 m plots and randomly took 12 soil cores to a depth of 20 cm from each plot using an 8 cm diameter auger. All soil cores from each plot were thoroughly mixed to form a composite sample, packed in paper sampling bags and immediately transported back to the laboratory. The soil samples were gently passed through a 2 mm sieve to remove visible plant tissues, animals, and stones and separated into two portions. One portion was air-dried and used for physicochemical analysis, and the other portion of the fresh soil was immediately stored in a refrigerator at 4 °C until the incubation experiment. The initial soil pH, total C, and total N were 5.4, 32.5, and 4.3 g kg^{-1}, respectively.

2.2. Microcosm setup

To test the effect of different electron acceptors on methane oxidation from paddy soils, we set up an anaerobic microcosm experiment. We placed fresh soil (~15 g of air-dried soil) in a 120 ml serum bottle, added 20 ml of sterile anaerobic distilled water, and mixed it to form a slurry. It was sealed with a high-temperature sterilized neoprene septum and an aluminum cap, and then repeatedly flushed with helium to ensure anoxic conditions were established. 36 such bottles were pre-incubated statically at 25 °C for 30 days to reduce the presence of the original electron acceptors such as nitrate, sulfate, and ferric iron. After pre-incubation, for each of the labeled tests, 20 ml of headspace gas was replaced with either an equal volume of $^{13}CH_4$ (Sigma-Aldrich, 99 atom % ^{13}C, USA) or with $^{12}CH_4$ as a reference. Six treatments were set up: (i) the negative control without addition any of electron acceptor, named the control (CK), (ii) Fe^{3+} (10 mM Ferrihydrite) (Fh), (iii) NO_3^- (5 mM $NaNO_3$) (N), (iv) Biochar (1%, w/w) (B), (v) Fe^{3+} (10 mM Ferrihydrite) + Biochar (1%, w/w) (FhB), (vi) NO_3^- (5 mM $NaNO_3$) + Biochar (1%, w/w) (NB). Three replicates were set up for each treatment. The vials were cultured at 25 °C in a shaking incubator at 150 rpm for 28 days.

The biochar used in this experiment was produced from air-dried rice stalks via slow pyrolysis at 460 °C in a muffle furnace (Isotemp, Fisher Scientific, USA) purged with N_2. The basic combustion process and properties of the derived biochar are shown in Table S1. Ferrihydrite was synthesized as described previously (Lovley and Phillips, 1986). Briefly, NaOH was added to neutralize $FeCl_3 \cdot 6H_2O$ to pH 7.0, then the precipitate was repeatedly washed with deionized water several times, freeze-dried, and stored in a sealed container.

2.3. CH_4 and $^{13}CO_2$ measurements

During the incubations, gas samples were collected at 1, 7, 14, 21, 28 days. A modified gas chromatograph (Agilent 7890A, Agilent, Palo Alto, CA, USA) equipped with a flame ionization detector (FID) was used to measure the methane concentration by injecting 100 μl samples. The temperatures of the oven, injection port, and detector were 60, 250, and 250 °C, respectively. The value of $^{13}CO_2$ was evaluated by a Delta V Advantage isotope ratio mass spectrometer (Thermo Fisher Scientific, Germany) with a calibrated CO_2 reference gas used to calculate the C isotope ratios.

2.4. DNA extraction and SIP gradient fractionation

After 28 days of incubation, the slurry samples were taken and freeze-dried. Total DNA was extracted from each sample of approximately 0.5 g freeze-dried soil using the FastDNA® SPIN Kit for Soil (MP Biomedicals, Cleveland, OH, USA) according to the manufacturer's instructions. A NanoDrop 2000 UV–vis spectrophotometer (Thermo Scientific, USA) was used to determine the concentration and quality after DNA extraction. DNA density gradient centrifugation and fractionation used our previously described method (Long et al., 2015). Briefly, 3 μg of DNA was mixed with 1.85 g ml^{-1} of CsCl solution and gradient buffer (0.1 M Tris-HCl, 0.1 M KCl, 1 mM EDTA, pH 8.0) to reach an initial CsCl buoyant density of 1.710 g ml^{-1}, which was determined by adjusting the refractive index to 1.4025 with an AR200 handheld refractometer (Reichert, New York, USA). A 5.1-ml Quick-Seal polyallomer ultracentrifugation tube (Beckman Coulter, Palo Alto, CA) with the above sample was centrifuged on an NVT 65.2 rotor (Beckman Coulter, USA) at 177,000 × *g* (45,000 rpm) for 44 h at 20 °C. Using sterile water injected into the top of the centrifuge tube, centrifuged gradients were fractionated into 15 equal volumes (~340 μl) by a single-channel syringe pump (LSP01-1A, Longer Precision Pump Co. Ltd., Baoding, China). Next, 120 μl liquor in each layer was sucked into the refractometer to measure the refractive index to determine the buoyant densities of the fractionated gradients. The procedure for fractionating DNA was: precipitation by 550 μl 30% polyethylene glycol (PEG) 6000 (30% PEG, 1.6 M NaCl), incubation for 2 h at room temperature, centrifugation at 13,000 ×*g* for 30 min, removal of the supernatant, addition of 500 μl 70% ethanol to wash twice, dissolution of the DNA in 30 μl nuclease-free water (Sigma-Aldrich, St. Louis, MO, USA), and storage at −20 °C.

2.5. Real-time PCR quantification and high-throughput sequencing

Real-time quantitative polymerase chain reaction (qPCR) of 15 gradient fractions for each treatment was performed with a Light Cycler Roche 480 instrument (Roche Molecular Systems, Switzerland) to determine the 16S rRNA genes according to the protocol described by Zhang et al. (2019). A negative control with distilled sterile water was also set up. A 10-fold serial dilution with known copy numbers of the standard samples was used to generate standard curves. The PCR amplification efficiencies were 89%–99%, with correlation coefficient (R^2) values greater than 0.99.

The universal primers 515F (5′-GTGCCAGCMGCCGCGGTAA-3′) and 806R (5′-GGACTACVSGGGTATCTAAT-3′) (Bates et al., 2011) were used to perform PCR amplification for sequencing of the V4 region from bacterial and archaeal 16S rRNA genes (approximately 250 nucleotides) by using an Illumina MiSeq System at the Majorbio Bio-Pharm Technology Co., Ltd. (Shanghai, China). Primers were tagged with unique 6-bp barcode sequences for each sample. The PCR cycling conditions were as follows: initial denaturation at 95 °C for 3 min, followed by 45 cycles of 95 °C for 15 s, 55 °C for 45 s and 72 °C for 45 s, and then 72 °C elongation for 5 min. The sequences were deposited into the NCBI sequence read archive (SRA) database with the accession number PRJNA 682286.

2.6. Data analysis

High-throughput sequencing data were analyzed using the Quantitative Insights into Microbial Ecology (QIIME) platform (version 1.9.0) (Caporaso et al., 2010). Briefly, raw data were de-multiplexed and quality controlled with the default setting in the QIIME pipeline. Reads with a Phred quality score (Q) < 20 and low-quality sequences (<50 bp) were discarded. The paired reads were merged with FLASH using default parameters. The putative chimeras were detected and removed by USEARCH (Edgar et al., 2011). Operational Taxonomic Units (OTUs) were clustered at 97% sequence similarity level by the UPARSE standard pipeline (Edgar, 2013). Taxonomy was assigned against representative sequences using the Ribosomal Database Project (RDP) Classifier (version 2.2, 0.8 confidence threshold) based on the SILVA 132 reference database (https://www.arb-silva.de/) (Wang et al., 2007; Quast et al., 2012) for bacterial and archaeal analyses. Principal Coordinate of

Analysis (PCoA) plots were processed by Origin 2019b software (Origin Lab Inc., USA) based on Bray-Curtis distance of OTUs, to compare the differences in community composition between the control and different electron acceptors. The PCoA plots were performed using the PERMANOVA test, and permutations were set to 999. The significantly different bacterial taxa in each cluster were determined by using the linear discriminant effect size (LEfSe) (Segata et al., 2011), conducted in Galaxy online (http://huttenhower.sph.harvard.edu/galaxy/). The linear discriminant analysis (LDA) scores of each group were greater than 3. A linear regression model was used to assess the relationship between the ^{13}C-labeled methane consumption and incubation time with the lm function performed in R studio software (version 4.0.2). The R package "ggplot2" was used for the visualization. All data were analyzed by Microsoft Excel 2010 software (Microsoft) and IBM SPSS Statistics 26 (IBM Inc., Chicago, IL, USA). Significant differences were analyzed using analysis of variance (ANOVA) followed by Tukey's honestly significant difference (HSD) test at $p \leq 0.05$.

3. Results

3.1. Methane consumption during the reduction of various electron acceptors

Over the 28 days of incubation, the methane concentration decreased to varying degrees with the addition of the different electron acceptors. The linear regression analysis of methane concentration at different time points (0, 1, 7, 14, 21, and 28 days) showed a high correlation based on $^{13}CH_4$ injection ($R^2 > 0.92$; Fig. S1). The rates of anaerobic oxidation of methane (AOM rates) were based on the slope given by the linear regression (Table 1). These rates ranged from 14.4 to 24.4 μg C g^{-1} dry soil d^{-1} and the ranking was CK ≈ B < Fh < N < NB < FhB. The addition of biochar had no significant effect on AOM rate, while the addition of NO_3^- and Fe^{3+} significantly increased AOM rates ($p < 0.05$).

3.2. $^{13}CO_2$ enrichment

We detected $^{13}CO_2$ enrichment derived from $^{13}CH_4$ with the various electron acceptors, presented as the isotope ratio, $^{13}F_{CO2}$ (calculated from $^{13}CO_2/(^{13}CO_2 + {}^{12}CO_2)$) (Fig. 1). The averages of $^{13}F_{CO2}$ during the 28 days are shown in Table 1. There was no significant difference between the control and the biochar treatment. The addition of nitrate and ferric iron significantly increased the rate of conversion of $^{13}CH_4$ to $^{13}CO_2$ compared to the control ($p < 0.05$). Moreover, the $^{13}CO_2$ enrichments of the FhB and NB treatments were slightly less than those of the single treatments (Fh and N), but the differences were not significant ($p > 0.05$).

In addition, to further demonstrate the occurrence of nitrate-dependent and iron-dependent AOM we performed a stoichiometry experiment (see Supplementary materials for details). The anaerobic methane oxidation (assessed as the oxidation of 585 μM $^{13}CH_4$ and production of 610 μM $^{13}CO_2$) was coupled to the reduction of nitrate ($^{15}NO_3^-$, 965 μM), with ^{15}N-N_2 as the main end-product (526 μM) (Fig. 2a). The stoichiometric ratio of $^{13}CH_4$ to $^{13}CO_2$ was 0.96, $^{15}NO_3^-$ to ^{15}N-N_2 was 1.83, and $^{13}CO_2$ to ^{15}N-N_2 was 1.16. The anaerobic methane oxidation (assessed as the oxidation of 578 μM $^{13}CH_4$ and production of 529 μM $^{13}CO_2$) was also coupled to the reduction of Fe^{3+} (5206 μM), with Fe^{2+} as the main end-product (5213 μM) (Fig. 2b). The stoichiometric ratio of $^{13}CH_4$ to $^{13}CO_2$ was 1.09, Fe^{3+} to Fe^{2+} was 1.00, and $^{13}CO_2$ to Fe^{2+} was 0.10. Accordingly, these results are in agreement with the theoretical values based on the above Eqs. (1) and (2).

Table 1
AOM rates and $^{13}CO_2$ enrichment with different electron acceptors after 28 days incubation after $^{13}CH_4$ injection.

	Treatment	AOM rate (μg C g^{-1} dry soil d^{-1})	$^{13}F_{CO2}$ ($^{13}CO_2/(^{12}CO_2 + {}^{13}CO_2)$)
1	CK	14.4^b	0.035^b
2	Fh	22.4^a	0.058^a
3	N	22.7^a	0.066^a
4	B	15.2^b	0.034^b
5	FhB	24.4^a	0.047^{ab}
6	NB	23.1^a	0.052^{ab}

Different letters above the numbers indicate significant differences ($p < 0.05$).

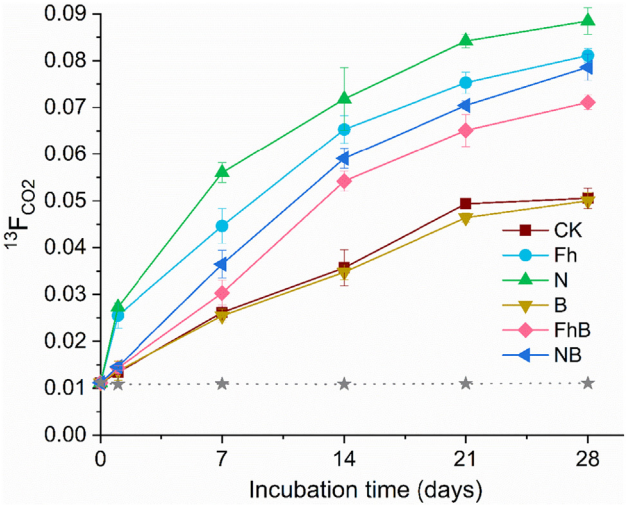

Fig. 1. $^{13}CO_2$ enrichment reported in $^{13}F_{CO2}$ ($^{13}CO_2/(^{13}CO_2 + {}^{12}CO_2)$) from $^{13}CH_4$ injection with various electron acceptors. The stars show the control with only $^{12}CH_4$ added. Error bars represent the range of the triplicate incubations.

3.3. DNA-SIP and microbial communities

Following DNA extraction and high-speed density gradient centrifugation, qPCR revealed the relative abundance contribution of 16S rRNA genes in each fraction (Fig. 3). It can be seen that the ^{13}C-labeled methane in each treatment has different degrees of deviation compared with the ^{12}C-methane, indicating that the density gradient of ^{13}C-labeled DNA (the "heavy" fractions) was from 1.71 to 1.73 g ml^{-1}, while ^{12}C-labeled DNA (the "light" fractions) was from 1.69 to 1.70 g ml^{-1}. The most obvious deviation was observed with the Fe^{3+} and Fe^{3+} + biochar treatments. However, the addition of biochar reduced the deviation of the NO_3^- treatment.

Based on the relative abundance distribution of 16S rRNA genes across the CsCl density gradients, 18 samples (6 treatments × 3 replicates) from the ^{13}C-treatment "heavy" fractions were chosen for sequencing and a total of 2,168,935 high-quality sequences were obtained. The relative distribution of bacteria and archaea at the phylum and genus levels were derived from the OTUs. The dominant bacterial phyla in the control were Firmicutes (71.35%), Proteobacteria (8.65%), and Actinobacteria (3.71%) (Fig. S2a). With the electron donor additions, the abundance of these three main phyla changed significantly compared with the control. Among these, the abundance of Firmicutes declined 5.89% with Fh, and 18.95% with FhB. However, the abundance of Proteobacteria and Actinobacteria increased 5.20% and 10.34% with Fh, and 5.08% and 3.30% with FhB, respectively. The N treatment significantly increased the content of Firmicutes, while the NB group slightly decreased the proportion of Firmicutes. Both N and NB increased the abundance of Proteobacteria. Moreover, the different electron acceptors increased the abundance of Bacteroidetes to varying degrees compared with the control. The relative distribution of bacteria at the genus level is shown in Fig. 4a. *Bacillus* was the most abundant bacterial genus in each treatment. Compared with CK, the content of *Bacillus* changed slightly in the B, N, and NB treatments, while the application of the Fh and FhB treatments significantly reduced it by nearly 50%. Notably, the supplementation by Fh increased the relative proportion of *Ammoniphilus*

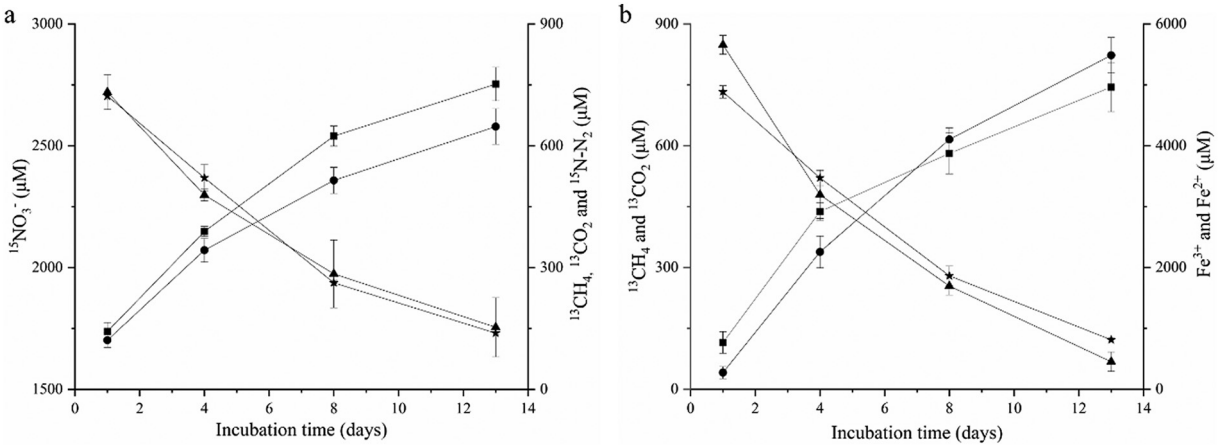

Fig. 2. (a) The stoichiometric analyses of $^{15}NO_3^-$ (triangles) reduction to ^{15}N-N_2 (circles) and $^{13}CH_4$ (stars) reduction to $^{13}CO_2$ (squares) in the presence of $^{13}CH_4$ in anaerobic slurry. (b) The stoichiometric analyses of Fe^{3+} (triangles) reduction to Fe^{2+} (circles) and $^{13}CH_4$ (stars) reduction to $^{13}CO_2$ (squares) in the presence of $^{13}CH_4$ in anaerobic slurry. The data are mean ± S.E. of three replicates.

and *Geobacter* by 329% and 640%, respectively, compared with CK. However, the abundance of these two genera only increased slightly in the FhB treatment and there was no significant change with the other three treatments. It should also be noted that with different electron acceptor additions, the abundance of *Planococcus* increased to different extents, especially in the N and NB treatments. We detected the three archaeal phyla, Euryarchaeota, Thaumarchaeota and Crenarchaeota, in all samples. Among them, Euryarchaeota and Crenarchaeota accounted for 39.41% and 14.50%, respectively, in CK, and the abundance of these two phyla increased to different degrees in the B, Fh, and N treatments. However, the abundances in the FhB and NB treatments were less than in CK (Fig. S2b). These variations with different treatments are not quite so obvious in the archaeal genera (Fig. S2c).

Principal coordinates analysis (PCoA) showed that the different treatments exhibited significantly different bacterial community structures ($p = 0.001$) (Fig. 4b). PCoA 1 and PCoA 2 accounted for 82% of the total variation. The Fh and FhB treatments were close in distance and far away from CK on both axes. The N, B, and NB treatments were close to each other and distant from CK but only on PCoA 2.

Accordingly, LEfSe analysis showed that significant taxonomic differences in bacteria occurred between different electron acceptor treatments (Fig. 5). The cladogram shows that the phylum Actinobacteria

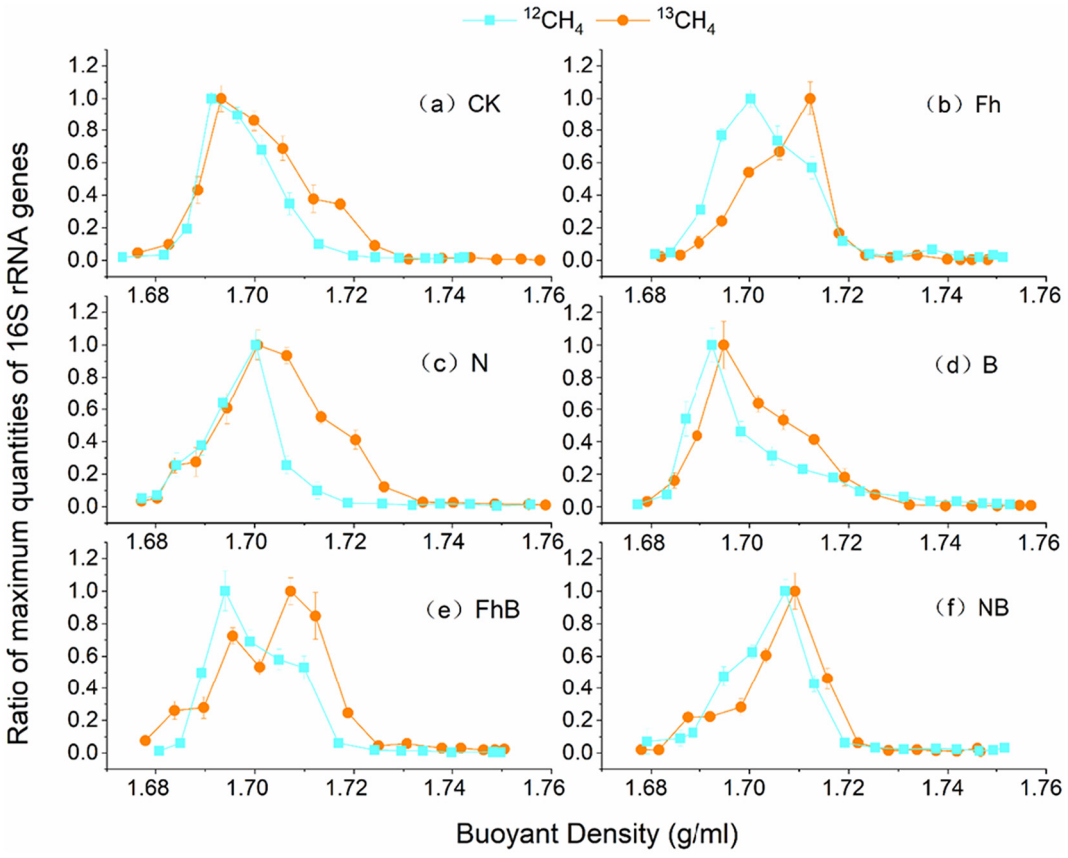

Fig. 3. The relative abundance distribution of 16S rRNA genes across the CsCl density gradients run for three replicates. Filled circles in orange represent ^{13}C-labeled methane, blue squares represent ^{12}C-methane.

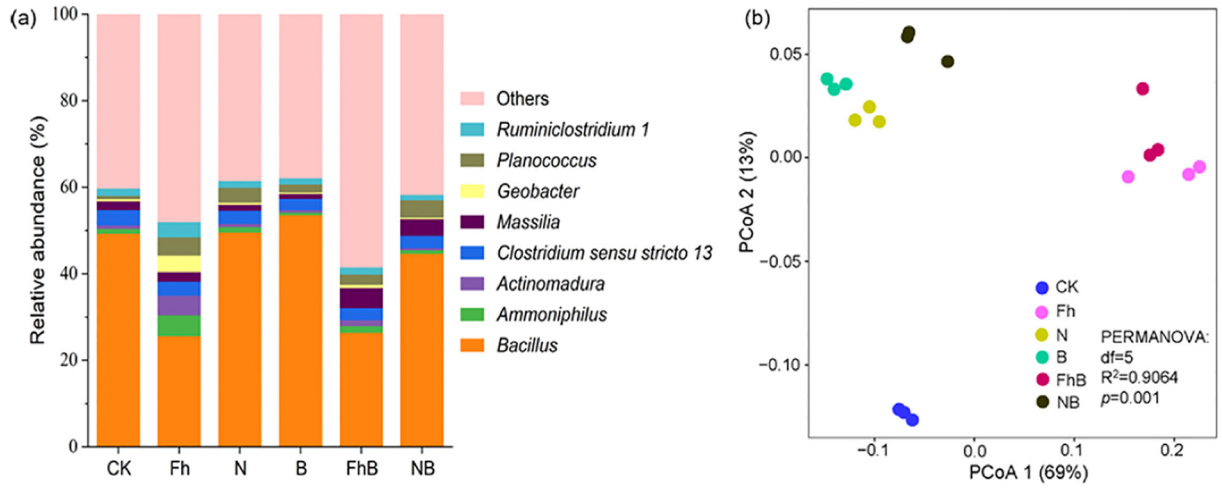

Fig. 4. Relative abundances of the main genera of bacteria, (a), and Principal coordinate analysis (PCoA) plot with Bray-Curtis dissimilarity, (b), between the different electron acceptor treatments.

was significantly more abundant in the Fh and FhB treatments. Among them, the class of Thermoleophilia was abundant in the FhB treatment, and Actinobacteria in the Fh treatment. The NB treatment was mainly defined by an increase in the phylum Bacteroidetes, while the N treatment showed a greater abundance of the class Bacilli and the genus *Rhodanobacter*. Additionally, the bacteria distinguishing the Fh treatment were mainly in the order Clostridiales. As for the B treatment, only the genus *Lysinibacillus* stood out. The heatmap analysis shows the differential microbes at the genus level for each sample (Fig. 6). Overall, the treatment with the most distinct bacterial community was Fh, followed by N, FhB, NB, B, and CK. Among them, *Geobacter*, *Ammoniphilus*, *Clostridium*, *Bacillus*, *Burkholderia*, and *Actinomadura* were enriched in the Fh treatment. *Rhodanobacter*, *Paenibacillus*, *Planococcus*, and *Tumebacillus* were enriched in the N treatment. Interestingly, when Fe^{3+} or NO_3^- was added with biochar, the abundance of these bacterial genera declined. With the addition of biochar alone (B), *Clostridium* sensu stricto 10 was enriched compared with CK.

4. Discussion

In this study, we investigated whether terminal electron acceptors (nitrate, ferric iron, and biochar) have a potentially positive effect on the anaerobic oxidation of methane, and what might be the related functional microorganisms. To clarify the effect of electron acceptors on the AOM process, we carried out an isotope labeling incubation (adding $^{13}CH_4$) to measure the AOM rate and related active microorganisms. The concentration of methane decreased while $^{13}CO_2$ increased to varying degrees after the addition of different electron acceptors in a strictly anaerobic environment (Figs. S1 and 1). Interestingly, there are differences in the curve trends (linear in Fig. S1 and asymptotic in Fig. 1). Here, we need to take into account the fact that a small amount of CH_4 and CO_2 is dissolved in water. Compared to CH_4, CO_2 is relatively soluble in water. Thus, a significant buildup of dissolved CO_2 might have occurred, which was not considered in gas phase measurements. Moreover, methanotrophs are able to assimilate CO_2 to varying degrees and may cause adverse effects on CO_2 concentrations (Strong et al., 2015). These factors may have caused the curve trend of $^{13}F_{CO2}$ to not be linear but asymptotic. Our results confirmed the presence of both nitrate-dependent and ferric iron-dependent AOM processes. With both nitrate and ferric iron reduction, the rate of AOM increased significantly, but biochar, which can also serve as a terminal electron acceptor, had no significant effect. Sequence analysis revealed different functional microorganisms that are likely to be involved in the AOM-terminal electronic acceptor coupling process.

In the present study, the AOM rate with the addition of Fe^{3+} and Fe^{3+} + biochar was significantly higher than in the CK and biochar groups, indicating that ferric iron-dependent AOM is a sink for methane, and could reduce the emission of methane, particularly in iron-rich paddy soils. Ferric iron-dependent AOM was first discovered in marine sediments (Beal et al., 2009) and has recently been found in many different environments. For example, Mohanty et al. (2017) reported that the redox reaction of iron in tropical soils (under soybeans and wheat) can stimulate methane oxidation by increasing the abundance of methanotrophs. Cai et al. (2018) found that the ANME archaea Candidatus '*Methanoperedens ferrireducens*' could use Fe^{3+} to mediate the AOM process. At the same time, Lu et al. (2018) supplemented a biofilm reactor with iron over a concentration gradient of 20–160 μM, and found a significant increase in the number of AOM bacteria and archaea. However, there has been no positive report about the coupling of iron reduction and AOM in paddy soil except for the work of Fan et al. (2020) who concluded that the role of iron was unclear. However, in line with most previous studies in other environments, we observed a significant reduction of CH_4 concentration after the addition of Fe^{3+} in our paddy soil. We suspect that the main reason why Fan et al. (2020) did not find this result might be the much lower concentration of ^{13}C-labeled methane they used as a recent study has shown that ferric iron-dependent AOM mainly occurs in environments with a high methane concentration (Shen et al., 2019).

The AOM process mediated by nitrate has the highest Gibbs free energy among the several electron acceptors that have been discovered. Hence we studied the role of nitrate in the AOM process and found that our result agrees with those of Vaksmaa et al. (2017), Shi et al. (2017) and Fan et al. (2020). Moreover, we combined the AOM rates with the $^{13}CO_2$ production rates through the labeling method and more clearly confirmed the role of nitrate. As shown in Fig. 1, the $^{13}CO_2$ enrichment in the nitrate treatment was the most abundant, which also identified a potentially relevant methane oxidation mechanism in paddy soil. It is worth noting that nitrite has also been shown to be used as an electron acceptor for AOM in paddy systems (Wang et al., 2012; Hu et al., 2014; Zhou et al., 2014). However, nitrate is the more natural input to paddy soil and is readily reduced to nitrite by other microorganisms such as the archaea 'Candidatus *Methanoperedens nitroreducens*' (Vaksmaa et al., 2017).

Regarding biochar, known to be an extracellular electron acceptor or shuttle, it showed no significant effect on CH_4 emission and $^{13}CO_2$ enrichment in our study. This is in accordance with Zhu et al. (2018) who found biochar addition (1%, w/w) did not affect methane emission in a 120-day anaerobic incubation. Unlike our study, some previous trials showed that biochar addition can

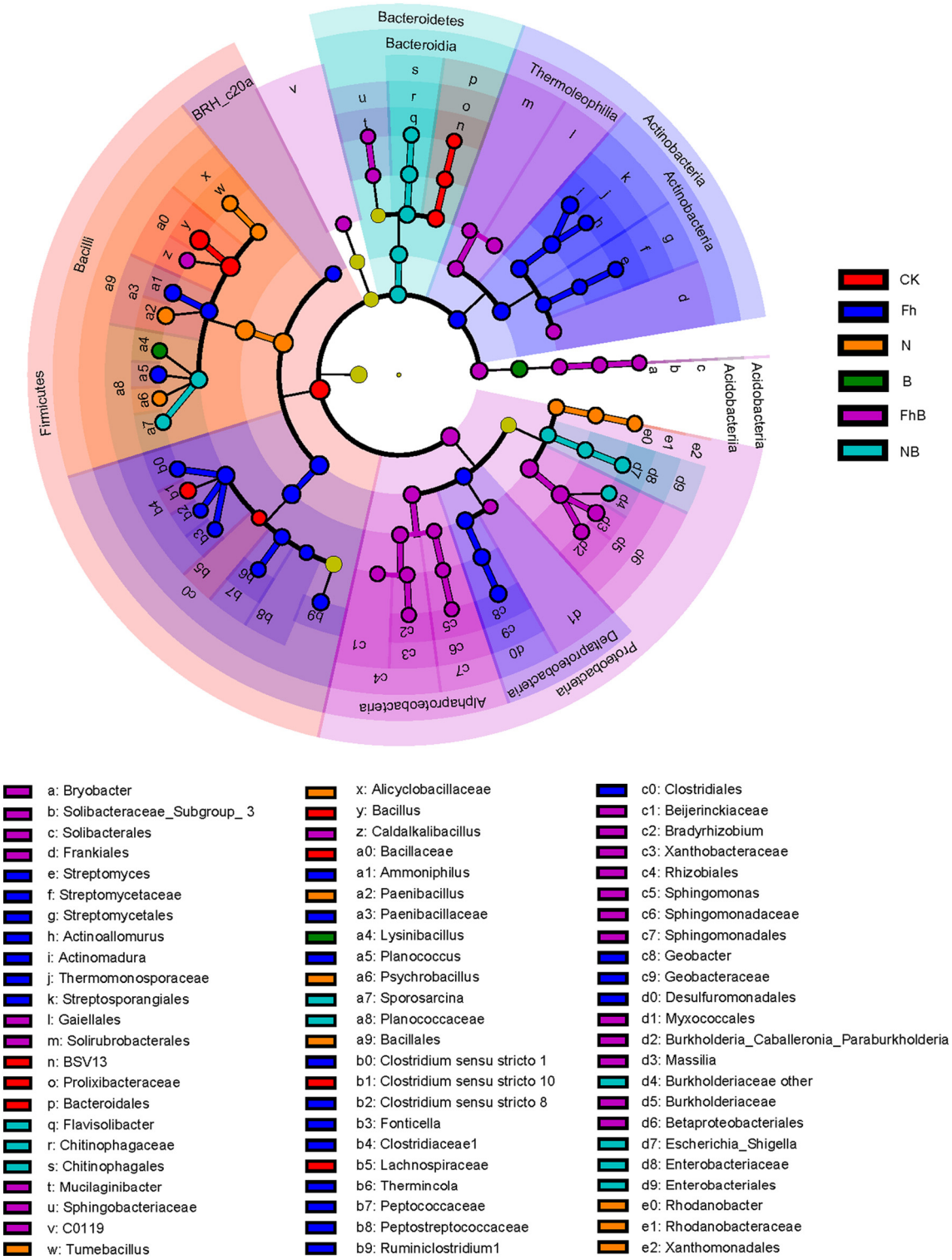

Fig. 5. Taxonomic cladogram derived from LEfSe analysis of the 16S sequences.

suppress CH_4 emissions in paddy soils (Feng et al., 2012; Nan et al., 2020) while others showed increased emissions (Ji et al., 2020). The reason for the reduction of methane emission reported by Nan et al. (2020) was that biochar increased soil aeration so that the aerobic methanotroph abundance increased significantly. However, our experiment was performed under strict anaerobic conditions, so it could not promote the abundance of methanotrophs requiring oxygen. Some studies have proposed the possibility that biochar acts as an electron shuttle; whether the electrons it accepts can be transferred to iron minerals or denitrifying bacteria is not clear-cut (Cayuela et al., 2013; Xu et al., 2013). We found iron and nitrate participate in the AOM process through a reduction reaction, but biochar does not promote this reduction process. Thus, biochar may be unable to transfer electrons to iron minerals or denitrifying bacteria. The specific mechanism of biochar as an electron shuttle remains to be studied further.

Based on DNA-SIP combined with high-throughput sequencing technology, we have identified the functional microorganisms promoted by

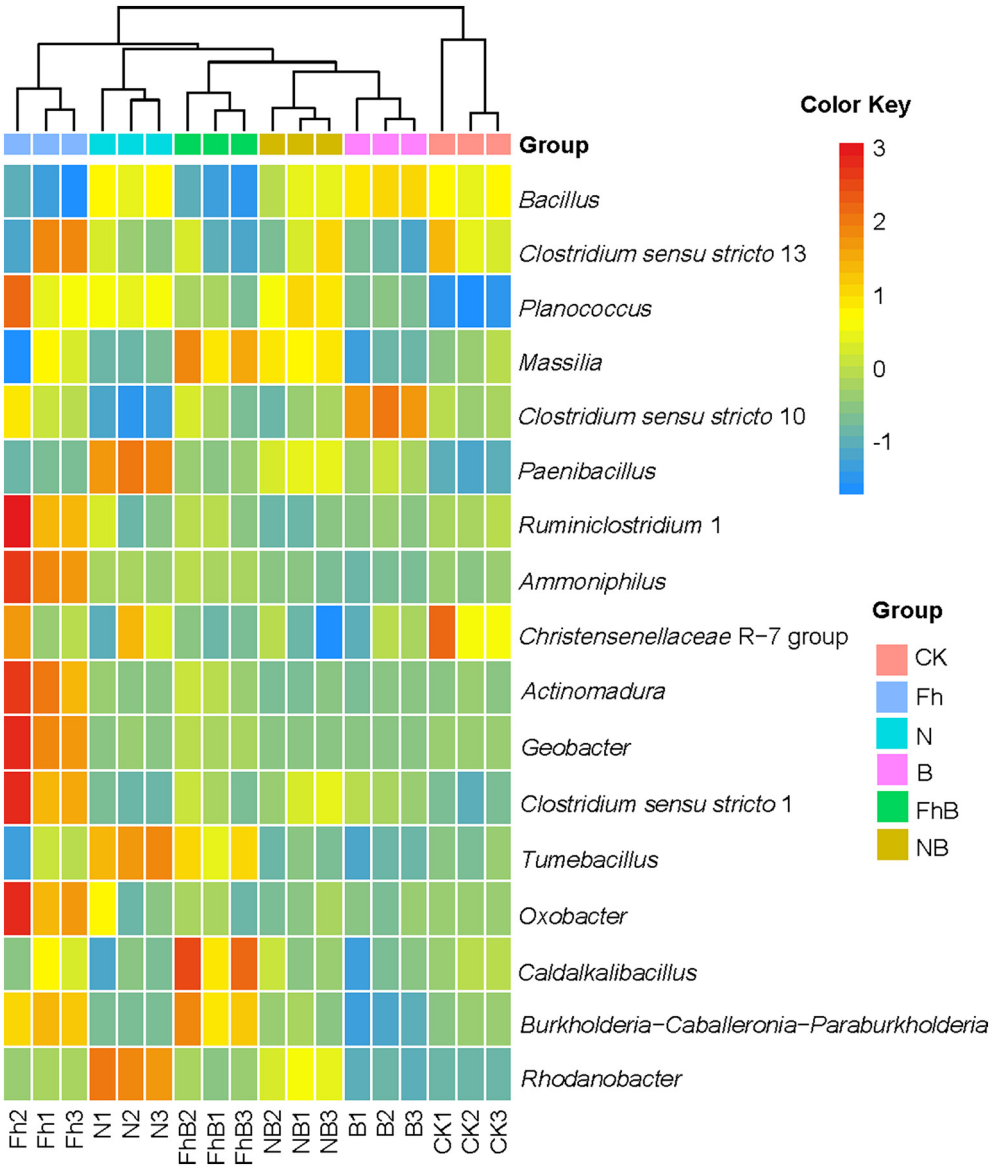

Fig. 6. Heatmap of genera in the relative abundances of bacterial communities in all treatments.

different electron receptors. Ferric iron, nitrate and biochar all had a significant impact on the microbial community. In our study, iron-reducing bacteria such as *Geobacter*, *Ammoniphilus* and *Clostridium* played a very important regulatory role for AOM in the paddy soil. A similar pattern of results was obtained in constructed wetland matrix systems with added iron oxide where it was found that dissimilatory metal-reducing bacteria (DMRB) can promote the reduction of iron oxides, thereby promoting AOM (Cheng et al., 2021). In previous studies, the archaea 'Candidatus *Methanoperedens nitroreducens*' and the bacteria NC10 phylum were the main microorganisms in nitrate-dependent AOM (Raghoebarsing et al., 2006; Vaksmaa et al., 2017). However, in the present study, some microorganisms related to nitrate reduction, such as *Rhodanobacter*, *Paenibacillus* and *Planococcus* which can be involved in denitrification or act as nitrate-reducing bacteria (Green et al., 2012; Chen et al., 2016; Latham et al., 2019), were found to be enriched in the AOM process following nitrate addition. In the LEfSe analysis, the distinguishing bacteria in the biochar treatment was *Lysinibacillus*, which is reported to have significantly improved the solubilization of phosphorus in biochar (He et al., 2014). However, biochar reduced the abundance of iron-reducing bacteria and nitrate-reducing bacteria, which may be due to the adsorption of Fe^{3+} and NO_3^- by the biochar. Different from the bacterial communities, changes in archaeal communities were not evident. It is important to bear in mind that the DNA-SIP discrimination of ^{12}C and ^{13}C is only partial and there is some overlap (Fig. 3). Thus, some ^{12}C-derived organisms could be present in the heavy fractions analyzed.

We were able to confirm the key roles of iron and nitrate in AOM in paddy soil. Ferric iron is the most abundant mineral oxide and nitrate-based fertilizers are prevalent in paddy soil (Xu et al., 2019). Both of them can act as terminal electron acceptors and promote AOM through their reduction, thus mitigating methane emissions and playing an important role in the geochemical cycle and global climate improvement. Previous studies on the AOM process mostly focused on the description of the correlation between the AOM rates and the number of microorganisms However, it is difficult to directly locate the active microorganisms. In this study, we used DNA-SIP combined with high-throughput sequencing technology to more specifically identify the microorganisms that participate in the AOM process with different electron receptors. It provides feasible guidance for the study of other processes within AOM. Although this study confirmed the active microorganisms of ferric iron-dependent AOM and nitrate-dependent AOM in paddy soils, further studies (e.g., isolation experiments, high-throughput sequencing of

mcrA and *pmoA* genes related to the production and consumption of CH_4) could be considered to substantiate this view.

5. Conclusions

In this paper, we have found ferric iron and nitrate act as terminal electron acceptors that can promote the oxidation of CH_4 to CO_2 and thus effectively mitigate the greenhouse gas emission in paddy soil. Furthermore, this work provides DNA-SIP based evidence that ferric iron-dependent AOM and nitrate-dependent AOM are mainly driven by iron-reducing bacteria and nitrate-reducing bacteria, respectively. Our results also suggest that biochar can be applied to paddy soil without causing changes to anaerobic methane oxidation. For future work, the exploration of other potential electron acceptors and related active microorganisms may be helpful to understanding the global geochemical cycle and the regulation of methane emissions.

CRediT authorship contribution statement

Dan Luo: Conceptualization, Investigation, Visualization, Data curation, Writing – original draft. **Huaiying Yao**: Methodology, Supervision, Writing – review & editing, Project administration, Funding acquisition, Validation. **Xiangtian Meng** and **Ningguo Zheng**: Supervision, Writing – review & editing. **Yaying Li**: Methodology, Supervision, Project administration. **Stephen J. Chapman**: Supervision, Writing – review & editing, Methodology.

Declaration of competing interest

The authors declare that they have no known competing financial interests or personal relationships that could have appeared to influence the work reported in this paper.

Acknowledgements

This work was supported by the National Natural Science Foundation of China [Grant Numbers 42077036, 42021005], the National Key R & D Program of China [Grant Number 2020YFC1806900], and Ningbo Municipal Science and Technology Bureau (202002N3079).

Appendix A. Supplementary data

Supplementary data to this article can be found online at https://doi.org/10.1016/j.scitotenv.2021.147773.

References

Achtnich, C., Bak, F., Conrad, R., 1995. Competition for electron donors among nitrate reducers, ferric iron reducers, sulfate reducers, and methanogens in anoxic paddy soil. Biol. Fertil. Soils 19, 65–72. https://doi.org/10.1007/BF00336349.

Bar-Or, I., Elvert, M., Eckert, W., Kushmaro, A., Vigderovich, H., Zhu, Q., Ben-Dov, E., Sivan, O., 2017. Iron-coupled anaerobic oxidation of methane performed by a mixed bacterial-archaeal community based on poorly reactive minerals. Environ. Sci. Technol. 51, 12293–12301. https://doi.org/10.1021/acs.est.7b03126.

Bates, S.T., Berg-Lyons, D., Caporaso, J.G., Walters, W.A., Knight, R., Fierer, N., 2011. Examining the global distribution of dominant archaeal populations in soil. ISME J. 5, 908–917. https://doi.org/10.1038/ismej.2010.171.

Batool, A., Taj, S., Rashid, A., Khalid, A., Qadeer, S., Saleem, A.R., Ghufran, M.A., 2015. Potential of soil amendments (biochar and gypsum) in increasing water use efficiency of Abelmoschus esculentus L. Moench. Front. Plant Sci. 6. https://doi.org/10.3389/fpls.2015.00733.

Beal, E.J., House, C.H., Orphan, V.J., 2009. Manganese- and iron-dependent marine methane oxidation. Science 325, 184–187. https://doi.org/10.1126/science.1169984.

Cai, C., Leu, A.O., Xie, G., Guo, J., Feng, Y., Zhao, J., Tyson, G.W., Yuan, Z., Hu, S., 2018. A methanotrophic archaeon couples anaerobic oxidation of methane to Fe(III) reduction. ISME J. 12, 1929–1939. https://doi.org/10.1038/s41396-018-0109-x.

Caldwell, S.L., Laidler, J.R., Brewer, E.A., Eberly, J.O., Sandborgh, S.C., Colwell, F.S., 2008. Anaerobic oxidation of methane: mechanisms, bioenergetics, and the ecology of associated microorganisms. Environ. Sci. Technol. 42, 6791–6799. https://doi.org/10.1021/es800120b.

Caporaso, J.G., Kuczynski, J., Stombaugh, J., Bittinger, K., Bushman, F.D., Costello, E.K., Fierer, N., Peña, A.G., Goodrich, J.K., Gordon, J.I., Huttley, G.A., Kelley, S.T., Knights, D., Koenig, J.E., Ley, R.E., Lozupone, C.A., McDonald, D., Muegge, B.D., Pirrung, M., Reeder, J., Sevinsky, J.R., Turnbaugh, P.J., Walters, W.A., Widmann, J., Yatsunenko, T., Zaneveld, J., Knight, R., 2010. QIIME allows analysis of high-throughput community sequencing data. Nat. Methods 7, 335–336. https://doi.org/10.1038/nmeth.f.303.

Cayuela, M.L., Sánchez-Monedero, M.A., Roig, A., Hanley, K., Enders, A., Lehmann, J., 2013. Biochar and denitrification in soils: when, how much and why does biochar reduce N_2O emissions? Sci. Rep. 3, 1732. https://doi.org/10.1038/srep01732.

Chen, S., Rotaru, A.E., Shrestha, P.M., Malvankar, N.S., Liu, F., Fan, W., Lovley, D.R., 2014. Promoting interspecies electron transfer with biochar. Sci. Rep. 4, 5019. https://doi.org/10.1038/srep05019.

Chen, D., Wei, L., Zou, Z., Yang, K., Wang, H., 2016. Bacterial communities in a novel three-dimensional bioelectrochemical denitrification system: the effects of pH. Appl. Microbiol. Biotechnol. 100, 6805–6813. https://doi.org/10.1007/s00253-016-7499-3.

Cheng, S., Qin, C., Xie, H., Wang, W., Hu, Z., Liang, S., Feng, K., 2021. A new insight on the effects of iron oxides and dissimilated metal-reducing bacteria on CH_4 emissions in constructed wetland matrix systems. Bioresour. Technol. 320, 124296. https://doi.org/10.1016/j.biortech.2020.124296.

Davies, T.R., 1973. Isolation of bacteria capable of utilizing methane as a hydrogen donor in the process of denitrification. Water Res. 7, 575–579. https://doi.org/10.1016/0043-1354(73)90056-0.

Edgar, R.C., 2013. UPARSE: highly accurate OTU sequences from microbial amplicon reads. Nat. Methods 10, 996–998. https://doi.org/10.1038/nmeth.2604.

Edgar, R.C., Haas, B.J., Clemente, J.C., Quince, C., Knight, R., 2011. UCHIME improves sensitivity and speed of chimera detection. Bioinformatics 27, 2194–2200. https://doi.org/10.1093/bioinformatics/btr381.

Egger, M., Rasigraf, O., Sapart, C.J., Jilbert, T., Jetten, M.S.M., Röckmann, T., van der Veen, C., Bândă, N., Kartal, B., Ettwig, K.F., Slomp, C.P., 2015. Iron-mediated anaerobic oxidation of methane in brackish coastal sediments. Environ. Sci. Technol. 49, 277–283. https://doi.org/10.1021/es503663z.

Ettwig, K.F., Zhu, B., Speth, D., Keltjens, J.T., Jetten, M.S.M., Kartal, B., 2016. Archaea catalyze iron-dependent anaerobic oxidation of methane. Proc. Natl. Acad. Sci. 113, 12792–12796. https://doi.org/10.1073/pnas.1609534113.

Fan, L., Dippold, M.A., Ge, T., Wu, J., Thiel, V., Kuzyakov, Y., Dorodnikov, M., 2020. Anaerobic oxidation of methane in paddy soil: role of electron acceptors and fertilization in mitigating CH_4 fluxes. Soil Biol. Biochem. 141, 107685. https://doi.org/10.1016/j.soilbio.2019.107685.

Feng, Y., Xu, Y., Yu, Y., Xie, Z., Lin, X., 2012. Mechanisms of biochar decreasing methane emission from Chinese paddy soils. Soil Biol. Biochem. 46, 80–88. https://doi.org/10.1016/j.soilbio.2011.11.016.

Gabriel, G.V.M., Oliveira, L.C., Barros, D.J., Bento, M.S., Neu, V., Toppa, R.H., Carmo, J.B., Navarrete, A.A., 2020. Methane emission suppression in flooded soil from Amazonia. Chemosphere 250, 126263. https://doi.org/10.1016/j.chemosphere.2020.126263.

Green, S.J., Prakash, O., Jasrotia, P., Overholt, W.A., Cardenas, E., Hubbard, D., Tiedje, J.M., Watson, D.B., Schadt, C.W., Brooks, S.C., Kostka, J.E., 2012. Denitrifying bacteria from the genus *Rhodanobacter* dominate bacterial communities in the highly contaminated subsurface of a nuclear legacy waste site. Appl. Environ. Microbiol. 78, 1039–1047. https://doi.org/10.1128/AEM.06435-11.

He, H., Qian, T., Liu, W., Jiang, H., Yu, H., 2014. Biological and chemical phosphorus solubilization from pyrolytical biochar in aqueous solution. Chemosphere 113, 175–181. https://doi.org/10.1016/j.chemosphere.2014.05.039.

He, Q., Yu, L., Li, J., He, D., Cai, X., Zhou, S., 2019. Electron shuttles enhance anaerobic oxidation of methane coupled to iron(III) reduction. Sci. Total Environ. 688, 664–672. https://doi.org/10.1016/j.scitotenv.2019.06.299.

Hu, B.L., Shen, L.D., Lian, X., Zhu, Q., Liu, S., Huang, Q., He, Z.F., Geng, S., Cheng, D.Q., Lou, L.P., Xu, X.Y., Zheng, P., He, Y.F., 2014. Evidence for nitrite-dependent anaerobic methane oxidation as a previously overlooked microbial methane sink in wetlands. Proc. Natl. Acad. Sci. 111, 4495–4500. https://doi.org/10.1073/pnas.1318393111.

Ji, M., Zhou, L., Zhang, S., Luo, G., Sang, W., 2020. Effects of biochar on methane emission from paddy soil: focusing on DOM and microbial communities. Sci. Total Environ. 743, 140725. https://doi.org/10.1016/j.scitotenv.2020.140725.

Keiluweit, M., Nico, P.S., Johnson, M.G., Kleber, M., 2010. Dynamic molecular structure of plant biomass-derived black carbon (biochar). Environ. Sci. Technol. 44, 1247–1253. https://doi.org/10.1021/es9031419.

Knittel, K., Boetius, A., 2009. Anaerobic oxidation of methane: progress with an unknown process. Annu. Rev. Microbiol. 63, 311–334. https://doi.org/10.1146/annurev.micro.61.080706.093130.

Latham, E.A., Pinchak, W.E., Trachsel, J., Allen, H.K., Callaway, T.R., Nisbet, D.J., Anderson, R.C., 2019. *Paenibacillus* 79R4, a potential rumen probiotic to enhance nitrite detoxification and methane mitigation in nitrate-treated ruminants. Sci. Total Environ. 671, 324–328. https://doi.org/10.1016/j.scitotenv.2019.03.390.

Leu, A.O., Cai, C., McIlroy, S.J., Southam, G., Orphan, V.J., Yuan, Z., Hu, S., Tyson, G.W., 2020. Anaerobic methane oxidation coupled to manganese reduction by members of the Methanoperedenaceae. ISME J. 14, 1030–1041. https://doi.org/10.1038/s41396-020-0590-x.

Li, D., Song, L., Fang, H., Li, P., Teng, Y., Li, Y., Liu, R., Niu, Q., 2019a. Accelerated biomethane production rate in thermophilic digestion of cardboard with appropriate biochar: dose-response kinetic assays, hybrid synergistic mechanism, and microbial networks analysis. Bioresour. Technol. 290, 121782. https://doi.org/10.1016/j.biortech.2019.121782.

Li, J., Luo, C., Zhang, D., Cai, X., Jiang, L., Zhang, G., 2019b. Stable-isotope probing-enabled cultivation of the indigenous bacterium *Ralstonia* sp. strain M1, capable of degrading phenanthrene and biphenyl in industrial wastewater. Appl. Environ. Microbiol. 85. https://doi.org/10.1128/AEM.00511-19.

Long, X., Yao, H., Wang, J., Huang, Y., Singh, B.K., Zhu, Y., 2015. Community structure and soil pH determine chemoautotrophic carbon dioxide fixation in drained paddy soils. Environ. Sci. Technol. 49, 7152–7160. https://doi.org/10.1021/acs.est.5b00506.

Lovley, D.R., Phillips, E.J.P., 1986. Organic matter mineralization with reduction of ferric iron in anaerobic sediments. Appl. Environ. Microbiol. 51, 683–689. https://doi.org/10.1128/aem.51.4.683-689.1986.

Lu, Y., Fu, L., Li, N., Ding, J., Bai, Y., Samaras, P., Zeng, R.J., 2018. The content of trace element iron is a key factor for competition between anaerobic ammonium oxidation and methane-dependent denitrification processes. Chemosphere 198, 370–376. https://doi.org/10.1016/j.chemosphere.2018.01.172.

Lueders, T., Friedrich, M.W., 2002. Effects of amendment with ferrihydrite and gypsum on the structure and activity of methanogenic populations in rice field soil. Appl. Environ. Microbiol. 68, 2484–2494. https://doi.org/10.1128/aem.68.5.2484-2494.2002.

Martinez-Cruz, K., Leewis, M., Herriott, I.C., Sepulveda-Jauregui, A., Anthony, K.W., Thalasso, F., Leigh, M.B., 2017. Anaerobic oxidation of methane by aerobic methanotrophs in sub-Arctic lake sediments. Sci. Total Environ. 607–608, 23–31. https://doi.org/10.1016/j.scitotenv.2017.06.187.

Mohanty, S.R., Bandeppa, G.S., Dubey, G., Ahirwar, U., Patra, A.K., Bharati, K., 2017. Methane oxidation in response to iron reduction-oxidation metabolism in tropical soils. Eur. J. Soil Biol. 78, 75–81. https://doi.org/10.1016/j.ejsobi.2016.08.007.

Nan, Q., Wang, C., Wang, H., Yi, Q., Wu, W., 2020. Mitigating methane emission via annual biochar amendment pyrolyzed with rice straw from the same paddy field. Sci. Total Environ. 746, 141351. https://doi.org/10.1016/j.scitotenv.2020.141351.

Niemann, H., Losekann, T., de Beer, D., Elvert, M., Nadalig, T., Knittel, K., Amann, R., Sauter, E.J., Schluter, M., Klages, M., Foucher, J.P., Boetius, A., 2006. Novel microbial communities of the Haakon Mosby mud volcano and their role as a methane sink. Nature 443, 854–858. https://doi.org/10.1038/nature05227.

Norði, K.À., Thamdrup, B., Schubert, C.J., 2013. Anaerobic oxidation of methane in an iron-rich Danish freshwater lake sediment. Limnol. Oceanogr. 58, 546–554. https://doi.org/10.4319/lo.2013.58.2.0546.

Pachauri, R.K., Allen, M.R., Barros, V.R., Broome, J., Cramer, W., Christ, R., Church, J.A., Clarke, L., Dahe, Q., Dasgupta, P., 2014. Climate change 2014: synthesis report. Contribution of Working Groups I, II and III to the Fifth Assessment Report of the Intergovernmental Panel on Climate Change. IPCC.

Qiao, J., Li, X., Hu, M., Li, F., Young, L.Y., Sun, W., Huang, W., Cui, J., 2017. Transcriptional activity of arsenic-reducing bacteria and genes regulated by lactate and biochar during arsenic transformation in flooded paddy soil. Environ. Sci. Technol. 52, 61–70. https://doi.org/10.1021/acs.est.7b03771.

Quast, C., Pruesse, E., Yilmaz, P., Gerken, J., Schweer, T., Yarza, P., Peplies, J., Glöckner, F.O., 2012. The SILVA ribosomal RNA gene database project: improved data processing and web-based tools. Nucleic Acids Res. 41, D590–D596. https://doi.org/10.1093/nar/gks1219.

Raghoebarsing, A.A., Pol, A., De Passchoonen, K.V., Smolders, A.J.P., Ettwig, K.F., Rijpstra, W.I.C., Schouten, S., Damste, J.S.S., Den Camp, H.J.M.O., Jetten, M.S.M., 2006. A microbial consortium couples anaerobic methane oxidation to denitrification. Nature 440, 918–921. https://doi.org/10.1038/nature04617.

Reeburgh, W.S., 1976. Methane consumption in Cariaco Trench waters and sediments. Earth Planet. Sci. Lett. 28, 337–344. https://doi.org/10.1016/0012-821X(76)90195-3.

Saquing, J.M., Yu, Y., Chiu, P.C., 2015. Wood-derived black carbon (biochar) as a microbial electron donor and acceptor. Environ. Sci. Technol. Lett. 3, 62–66. https://doi.org/10.1021/acs.estlett.5b00354.

Scheller, S., Yu, H., Chadwick, G.L., McGlynn, S.E., Orphan, V.J., 2016. Artificial electron acceptors decouple archaeal methane oxidation from sulfate reduction. Science 351, 703–707. https://doi.org/10.1126/science.aad7154.

Segarra, K.E.A., Comerford, C., Slaughter, J., Joye, S.B., 2013. Impact of electron acceptor availability on the anaerobic oxidation of methane in coastal freshwater and brackish wetland sediments. Geochim. Cosmochim. Acta 115, 15–30. https://doi.org/10.1016/j.gca.2013.03.029.

Segarra, K.E.A., Schubotz, F., Samarkin, V., Yoshinaga, M.Y., Hinrichs, K., Joye, S.B., 2015. High rates of anaerobic methane oxidation in freshwater wetlands reduce potential atmospheric methane emissions. Nat. Commun. 6, 7477. https://doi.org/10.1038/ncomms8477.

Segata, N., Izard, J., Waldron, L., Gevers, D., Miropolsky, L., Garrett, W.S., Huttenhower, C., 2011. Metagenomic biomarker discovery and explanation. Genome Biol. 12, R60. https://doi.org/10.1186/gb-2011-12-6-r60.

Shen, L., Ouyang, L., Zhu, Y., Trimmer, M., 2019. Active pathways of anaerobic methane oxidation across contrasting riverbeds. ISME J. 13, 752–766. https://doi.org/10.1038/s41396-018-0302-y.

Shi, Y., Wang, Z., He, C., Zhang, X., Sheng, L., Ren, X., 2017. Using ^{13}C isotopes to explore denitrification-dependent anaerobic methane oxidation in a paddy-peatland. Sci. Rep. 7,40848. https://doi.org/10.1038/srep40848.

Shi, L., Guo, T., Lv, P., Niu, Z., Zhou, Y., Tang, X., Zheng, P., Zhu, L., Zhu, Y., Kappler, A., Zhao, H., 2020. Coupled anaerobic methane oxidation and reductive arsenic mobilization in wetland soils. Nat. Geosci. 13, 799–805. https://doi.org/10.1038/s41561-020-00659-z.

Sivan, O., Adler, M., Pearson, A., Gelman, F., Baror, I., John, S.G., Eckert, W., 2011. Geochemical evidence for iron-mediated anaerobic oxidation of methane. Limnol. Oceanogr. 56, 1536–1544. https://doi.org/10.4319/lo.2011.56.4.1536.

Song, B., Tang, J., Zhen, M., Liu, X., 2019. Influence of graphene oxide and biochar on anaerobic degradation of petroleum hydrocarbons. J. Biosci. Bioeng. 128, 72–79. https://doi.org/10.1016/j.jbiosc.2019.01.006.

Strong, P.J., Xie, S., Clarke, W.P., 2015. Methane as a resource: can the methanotrophs add value? Environ. Sci. Technol. 49, 4001–4018. https://doi.org/10.1021/es504242n.

Sun, J., Wang, M., Xu, X., Cheng, K., Yue, Q., Pan, G., 2020. Re-estimating methane emissions from Chinese paddy fields based on a regional empirical model and high-spatial-resolution data. Environ. Pollut. 265, 115017. https://doi.org/10.1016/j.envpol.2020.115017.

Vaksmaa, A., Guerrero-Cruz, S., van Alen, T.A., Cremers, G., Ettwig, K.F., Lüke, C., Jetten, M.S.M., 2017. Enrichment of anaerobic nitrate-dependent methanotrophi 'Candidatus *Methanoperedens nitroreducens*' archaea from an Italian paddy field soil. Appl. Microbiol. Biotechnol. 101, 7075–7084. https://doi.org/10.1007/s00253-017-8416-0.

Wang, Q., Garrity, G.M., Tiedje, J.M., Cole, J.R., 2007. Naïve bayesian classifier for rapid assignment of rRNA sequences into the new bacterial taxonomy. Appl. Environ. Microbiol. 73, 5261–5267. https://doi.org/10.1128/AEM.00062-07.

Wang, Y., Zhu, G., Harhangi, H., Zhu, B., Jetten, M.S.M., Yin, C., Camp, H.J.M.O., 2012. Co-occurrence and distribution of nitrite-dependent anaerobic ammonium and methane-oxidizing bacteria in a paddy soil. FEMS Microbiol. Lett. 336, 79–88. https://doi.org/10.1111/j.1574-6968.2012.02654.x.

Xu, X., Cao, X., Zhao, L., 2013. Comparison of rice husk- and dairy manure-derived biochars for simultaneously removing heavy metals from aqueous solutions: role of mineral components in biochars. Chemosphere 92, 955–961. https://doi.org/10.1016/j.chemosphere.2013.03.009.

Xu, J., Li, X., Sun, G., Cui, L., Ding, L., He, C., Li, L., Shi, Q., Smets, B.F., Zhu, Y., 2019. Fate of abile organic carbon in paddy soil is regulated by microbial ferric iron reduction. Environ. Sci. Technol. 53, 8533–8542. https://doi.org/10.1021/acs.est.9b01323.

Yan, X., Akiyama, H., Yagi, K., Akimoto, H., 2009. Global estimations of the inventory and mitigation potential of methane emissions from rice cultivation conducted using the 2006 Intergovernmental Panel on Climate Change Guidelines. Glob. Biogeochem. Cycles 23. https://doi.org/10.1029/2008GB003299.

Zhang, M., Wang, J., Bai, S.H., Zhang, Y., Teng, Y., Xu, Z., 2019. Assisted phytoremediation of a co-contaminated soil with biochar amendment: contaminant removals and bacterial community properties. Geoderma 348, 115–123. https://doi.org/10.1016/j.geoderma.2019.04.031.

Zhang, S., Zhang, Z., Xia, S., Ding, N., Long, X., Wang, J., Chen, M., Ye, C., Chen, S., 2020. Combined genome-centric metagenomics and stable isotope probing unveils the microbial pathways of aerobic methane oxidation coupled to denitrification process under hypoxic conditions. Bioresour. Technol. 318, 124043. https://doi.org/10.1016/j.biortech.2020.124043.

Zhou, L., Wang, Y., Long, X., Guo, J., Zhu, G., 2014. High abundance and diversity of nitrite-dependent anaerobic methane-oxidizing bacteria in a paddy field profile. FEMS Microbiol. Lett. 360, 33–41. https://doi.org/10.1111/1574-6968.12567.

Zhu, M., Zhang, L., Zheng, L., Zhuo, Y., Xu, J., He, Y., 2018. Typical soil redox processes in pentachlorophenol polluted soil following biochar addition. Front. Microbiol. 9, 579. https://doi.org/10.3389/fmicb.2018.00579.

Zhu, Y., Li, Y., Zheng, N., Chapman, S.J., Yao, H., 2020. Similar but not identical resuscitation trajectories of the soil microbial community based on either DNA or RNA after flooding. Agronomy 10, 502. https://doi.org/10.3390/agronomy10040502.